Transition in pipe flow: the saddle structure on the boundary of turbulence

Y. DUGUET,[1] A.P. WILLIS[1]
AND R.R. KERSWELL[1]

[1] School of Mathematics, University of Bristol, BS8 1TW Bristol, United Kindgdom.

(Received November 13th 2007 and in revised form ??)

The laminar-turbulent boundary Σ is the set separating initial conditions which immediately relaminarise from those which lead to turbulence. Phase space trajectories on this hypersurface in cylindrical pipe flow are chaotic and show recurring evidence of coherent structures. A general numerical technique is developed for recognising near-visits to these structures and then for identifying the exact coherent solutions themselves. Numerical evidence is presented which suggests that trajectories on Σ are organised around only a few travelling waves and their heteroclinic connections. If the flow is suitably constrained to a subspace with a discrete rotational symmetry, it is possible to find locally-attracting travelling waves embedded within Σ. Using this technique, 5 new travelling wave branches were found.

1. Introduction

Transition to turbulence in cylindrical pipe flow is governed by one single dimensionless parameter, the Reynolds number $Re := UD/\nu$ where U is the mean flow speed along the pipe, D the pipe diameter and ν the kinematic viscosity of the fluid (Reynolds 1883). Despite the simplicity of the set-up, the reason for transition remains obscure due to the sensitivity of the linearly-stable laminar Hagen-Poiseuille flow (Hagen 1839, Poiseuille 1840) to the shape and amplitude of disturbances. In most experiments, transition is observed at $Re \sim 2000$ (e.g. Wygnanski & Champagne 1973) but can be triggered as low as $Re = 1750$ (Peixinho & Mullin 2006) or delayed to $Re = 100,000$ in very carefully controlled experiments (Pfenniger 1961). Until recently, the only firm theoretical result was the energy stability bound of $Re = 81.49$ (Joseph & Carmi, 1969) below which *all* disturbances are guaranteed to decay monotonically. This is, however, more than an order of magnitude below the observed value for transition.

An important step forward in understanding the transition process was the discovery of disconnected solutions of the Navier-Stokes equations in an axially-periodic pipe (Faisst & Eckhardt 2003, Wedin & Kerswell 2004, Kerswell 2005). These exact solutions are travelling waves (TWs) which appear through saddle-node bifurcations. All these solutions are linearly unstable but have a very low-dimensional unstable manifold. There is an interest in these solutions as very similar structures have been observed transiently in experiments (Hof et al. 2004) and direct numerical simulations (Willis & Kerswell 2007). These states can generally be divided into "lower-branch" and "upper-branch" TWs, based on whether they have high or low wall friction factor. Lower branch solutions are believed to sit on a hypersurface that divides phase space into two regions: one where initial conditions lead directly to the laminar state, the other where initial

conditions lead to turbulent transients with larger kinetic energy (Kerswell & Tutty 2007 and in plane Couette flow, Kawahara 2005, Viswanath 2007b). The simple translational behaviour of these travelling wave solutions is inherent to the method used to find them, and undoubtedly masks an even larger variety of more complex exact solutions.

The boundary between laminar and turbulent trajectories - labelled Σ or called the "edge" following Skufca et al. (2006) hereafter - is formally a separatrix if the turbulent state is an attractor. At low Re, however, turbulence may ultimately decay after a long transient in which case the laminar state is the unique global attractor. Then the boundary Σ is generalised to the dividing set in phase space between trajectories which immediately (and smoothly) relaminarise and those which undergo some form of turbulent evolution. Σ is thought to be of codimension 1 in phase space but one can *a priori* not exclude a more complex fractal structure, as suggested by the dependence of lifetime on initial conditions in simulations of low-order models of pipe flow (Faisst & Eckhardt 2004). Trajectories which start in Σ, stay in Σ for later times by definition and hence the long time dynamics are of obvious interest. The long time behaviour on Σ has already been found to be a periodic orbit in plane Poiseuille flow in a pioneering study by Toh & Itano (1999,2001,2003). Skufca et al. (2006) studied a 9-dimensional model of plane Couette flow (PCF) to reveal an attracting periodic orbit at low Re and a chaotic state at higher Re. However, recent fully-resolved simulations have shown that the asymptotic behaviour is an attracting TW in PCF (Lagha et al. 2008) and a chaotic attractor in a short cylindrical pipe of length $L = 5D$ (Schneider et al. 2007). Interestingly, this chaotic endstate looks to be centred around a known asymmetric TW (Pringle & Kerswell 2007, Meseguer & Mellibovsky 2007).

The purpose of this paper is to explore the dividing hypersurface Σ in pipe flow with the following objectives:

(a) to establish that the dynamics restricted to this laminar-turbulent boundary explores many different saddle points embedded in it;
(b) to find evidence for heteroclinic or "relative" homoclinic connections between these saddle points;
(c) to explore Σ restricted by a discrete rotational symmetry in order to ascertain whether the limiting behaviour remains chaotic or can be a simple attractor;
(d) to develop a practical and general way to find TWs and periodic orbits without detailed knowledge of their spatial structure.

This paper is organised as follows. Section 2 discusses the formulation and numerical methods used to simulate the flow in a pipe and to extract exact recurrent flow solutions. Section 3 presents the results obtained using these in 6 subsections. Subsection 3.1 recalls the method used to follow trajectories on Σ and confirms that the limiting behaviour is chaotic (Schneider et al. 2007). §3.2 and §3.3 discuss how near-recurrent states are identified, and using a Newton-Krylov algorithm, demonstrate that a number of unstable travelling waves are embedded in Σ. §3.4 shows the existence of a "relative" homoclinic connection between a travelling wave and the same wave rotated. Recurrent flow structures are sought embedded within Σ restricted by a discrete rotational symmetry in §3.5 and new exact travelling wave solutions subsequently identified. §3.6 shows that within this subspace the limiting state of Σ is a simple attractor before the paper ends with a discussion in section 4.

2. Numerical Procedure

2.1. *Governing Equations*

We consider the incompressible flow of Newtonian fluid in a cylindrical pipe and adopt the usual set of cylindrical coordinates (s, θ, z) and velocity components $\boldsymbol{u} = u\hat{\boldsymbol{s}}+v\hat{\boldsymbol{\theta}}+w\hat{\boldsymbol{z}}$. The domain considered here is $(s, \theta, z) \in [0:1] \times [0:2\pi] \times [0:L]$, where $L = 2\pi/\alpha$ is the length of the pipe and lengths are in units of radii $(D/2)$. The flow is described by the incompressible three-dimensional Navier-Stokes equations

$$\frac{\partial \boldsymbol{u}}{\partial t} + (\boldsymbol{u} \cdot \boldsymbol{\nabla})\, \boldsymbol{u} = -\boldsymbol{\nabla} p + \frac{1}{Re}\nabla^2 \boldsymbol{u}, \tag{2.1}$$

$$\boldsymbol{\nabla} \cdot \boldsymbol{u} = 0, \tag{2.2}$$

and the flow is driven by a constant mass-flux condition, as in recent experiments (e.g. Peixinho & Mullin 2006). The boundary conditions are periodicity across the pipe length $\boldsymbol{u}(s, \theta, z) = \boldsymbol{u}(s, \theta, z + L)$ and no-slip on the walls $\boldsymbol{u}(1, \theta, z) = \boldsymbol{0}$.

2.2. *Time-stepping code*

The basic tool for the numerical determination of exact recurrent states is the accurate time-stepping code described by Willis & Kerswell (2007). The velocity field is derived from two scalar potentials Ψ and Φ

$$\boldsymbol{u} = \boldsymbol{\nabla} \times (\Psi \hat{z}) + \boldsymbol{\nabla} \times \boldsymbol{\nabla} \times (\Phi \hat{z}) \tag{2.3}$$

and the incompressible Navier-Stokes equations are rewritten using the formulation introduced by Marqués (1990). The two scalar potentials are discretised using high-order finite differences in the radial direction s and spectral Fourier expansions in the azimuthal direction θ and axial direction z. For example, the decomposition of the scalar potential Φ at a radial location s_j, $(j = 1, ..., N)$, reads

$$\Phi(s_j, \theta, z, t; \alpha, m_0) = \sum_{k=-K}^{K} \sum_{m=-M}^{M} \Phi_{jkm}(t) e^{i(m_0 m\theta + \alpha k z)}. \tag{2.4}$$

The positive integer m_0 refers to the discrete rotational symmetry

$$R_{m_0} : (u, v, w, p)(s, \theta, z) \to (u, v, w, p)(s, \theta + \frac{2\pi}{m_0}, z) \tag{2.5}$$

of the flow ($m_0 = 1$ means no rotational symmetry is imposed). The resolution of a given calculation is described by a vector (N, M, K). It is adjusted until the energy spectrum drops by at least 4 decades from lowest to highest-order modes. The corresponding number of (real) degrees of freedom, which defines the dimension of phase-space, is $O(8MNK)$. The set of all complex coefficients $\boldsymbol{X} = \{\Phi_{jkm}, \Psi_{jkm}\}$ defines our phase-space with its usual Euclidean norm $|\boldsymbol{X}| = \sqrt{\boldsymbol{X} \cdot \boldsymbol{X}}$. Note that neither the shift-and-reflect symmetry

$$S : (u, v, w, p)(s, \theta, z) \to (u, -v, w, p)(s, -\theta, z + \frac{\pi}{\alpha}) \tag{2.6}$$

nor the mirror symmetry (e.g. Pringle & Kerswell 2007)

$$Z : (u, v, w, p)(s, \theta, z) \to (u, -v, w, p)(s, -\theta, z) \tag{2.7}$$

are imposed in the code. The time stepping is 2nd order accurate with Δt updated using an adaptive method based on a CFL condition.

2.3. *The Newton-Krylov method*

The spectral expansion defined above converts the Navier-Stokes equations into an autonomous dynamical system of the form

$$\frac{d\boldsymbol{X}}{dt} = \boldsymbol{F}(\boldsymbol{X}). \tag{2.8}$$

Travelling wave solutions are steady solutions of the Navier-Stokes in an appropriate Galilean frame (Wedin & Kerswell, 2004). As such they are a special case of a periodic orbit which itself is a particular type of a "relative periodic orbit" (RPO) (Viswanath 2007a,2007b). To maintain generality, we developed an algorithm to look for RPOs defined as zeros of the functional

$$g = |\boldsymbol{X}(T)^{-\Delta z,-\Delta\theta} - \boldsymbol{X}(0)|^2. \tag{2.9}$$

Here, $\boldsymbol{X}(T)$ is the point at time T on the trajectory starting at time $t = 0$ from the point $\boldsymbol{X}(0)$. $\boldsymbol{X}^{-\Delta z,-\Delta\theta}$ is the point in phase space corresponding to the state $\boldsymbol{X}$ shifted back in space by the distance Δz in the axial direction and by the angle $\Delta\theta$ in the azimuthal direction. A shift back by $(\Delta z, \Delta\theta)$ corresponds in phase-space to the transformation:

$$(\Psi_{jkm}, \Phi_{jkm}) \rightarrow (\Psi_{jkm}, \Phi_{jkm}) e^{-i(mm_0\Delta\theta + \alpha k \Delta z)}. \tag{2.10}$$

A zero of g corresponds to a flow repeating itself exactly after a time T, but at a different location defined by Δz and $\Delta\theta$. A travelling wave solution (or "relative equilibrium") is a special case of a RPO where there is a degeneracy between the shifts Δz and $\Delta\theta$, and the period T. For example, in the case of a TW propagating axially with speed c, $\Delta z = cT$, where T is the apparent period. To remove this degeneracy, we impose $\Delta z = L$. For most of the time, unless specified, $\Delta\theta = 0$ is assumed as the majority of the TWs found do not rotate. Starting from a good initial guess for $\boldsymbol{X}(0)$ and an estimate of the period T (to be discussed in Section 3.2), we minimise the residual g by a Newton-Krylov algorithm, based on a GMRES algorithm (Saad & Schultz, 1986). The size of the dynamical system (typically 10^5 degrees of freedom) necessitates the use of a matrix-free formulation. The use of an *inexact* Krylov solver also allowed for an important gain in computation time (Eisenstat & Walker, 1995). Moreover, we embed the Newton solver into a more globally convergent strategy in order to improve likeliness of convergence, by using a double dogleg step technique (Dennis & Schnabel, 1995, Viswanath 2007a). In the special case of TWs with a short period, we assume full convergence when the normalised residual $\sqrt{g}/|\boldsymbol{X}(0)|$ is less than $O(10^{-10})$.

2.4. *Stability of Travelling Waves*

Once a travelling wave solution is known, along with its axial propagation speed c, it can be expressed as a steady solution in the frame moving at speed c. In this Galilean frame, the stability of the solutions can be studied numerically using an eigenvalue solver based on an Arnoldi algorithm. This yields the leading eigenvalues whose real part, when positive, indicates the growth rate of infinitesimal perturbations to the exact solution in the moving frame.

3. Results

We present 4 'edge' calculations, each motivated by a different question. In the first (see §3.1, §3.2 and §3.3), the edge in a pipe of length $\approx 5\,D$ ($\alpha = 0.625$) is calculated starting from a general turbulent initial condition in order to investigate whether there are coherent structures buried in the edge. In the process, we are able to confirm the

presence of a chaotic attractor as found recently by Schneider et. al. (2007). In the second (§3.4), we look for numerical evidence of heteroclinic connections between saddle points by using a perturbed TW as an initial condition. In the third (§3.5), we impose the discrete rotational symmetry R_2 on the flow to exploit the saddle structure of the subset of Σ to reveal new TWs which possess R_2-symmetry. In the fourth (§3.6), we look for evidence of multiple attracting TWs to demonstrate that under a rotational symmetry constraint the large-time dynamics need not be chaotic.

3.1. *Calculating Edge Trajectories*

In this subsection we choose a pipe with $\alpha = 0.625$ and $Re = 2875$, set $m_0 = 1$ so that there is no restriction on the rotational symmetry, and take a numerical resolution of $(30, 15, 15)$. In order to constrain a numerical trajectory to stay on the edge surface Σ, we use a shooting method analogous to that used first in plane Poiseuille flow by Toh & Itano (1999,2001). We first produce a long turbulent trajectory and pick any state $\boldsymbol{u}^*$ of relatively low energy. We then define the state

$$\boldsymbol{u}_\beta := \langle\, \boldsymbol{u}^* \rangle + \beta(\boldsymbol{u}^* - \langle \boldsymbol{u}^* \,\rangle) \tag{3.1}$$

where β is a real positive number and $\langle \quad \rangle$ is either the azimuthal average $\langle \quad \rangle_\theta = \frac{1}{2\pi}\int_0^{2\pi}(..)d\theta$ or the axial average $\langle \quad \rangle_z = \frac{\alpha}{2\pi}\int_0^{\frac{2\pi}{\alpha}}(..)dz$. For either averaging, any trajectory starting from $\boldsymbol{u}_{\beta=0}$ leads to quick relaminarisation, since turbulence can only be triggered by three-dimensional disturbances. If $\boldsymbol{u}_\beta$ leads to high energy levels typical of turbulent transients, the value of β is reduced, whereas it is increased if relaminarisation occurs. Using a bisection method, β is refined up to 14 significant digits in double precision arithmetic, forcing the energy of the trajectory to stay at an intermediate level corresponding to the laminar-turbulent boundary or edge for typical times of $O(200\,D/U)$. The success of this approach rests on being able to qualitatively distinquish between laminar, intermediate and turbulent energy levels. Once the trajectory starts to leave the edge after a time $O(200\,D/U)$, the process is simply restarted from a state near the end of the previous trajectory on the boundary. The resulting trajectory, of duration $O(500\,D/U)$, does not show any sign of convergence towards any simple state but rather displays chaotic dynamics as found by Schneider et al (2007). We deliberately avoid the word 'turbulent' as this refers to more energetic dynamics. Figure 1 shows the chaotic time evolution of the energy contained in the axially-dependent modes ($k \neq 0$).

3.2. *Near-Recurrences on an Edge Trajectory*

Despite the lack of regularity of the energy signals, inspection of all velocity components at several arbitrary locations in the pipe indicate clearly that the flow on Σ is sometimes nearly periodic in time on short intervals. In the case $(\alpha, Re, m_0) = (0.625, 2875, 1)$, we can identify by eye several temporal windows where all velocity components oscillate approximately with a given frequency (see Figure 2). A large number of snapshots were taken at times $t_i, i = 1, 2, 3...$ across the whole trajectory. To investigate the possibility of recurrence in the flow, each snapshot state $\boldsymbol{X}(t_i)$ was used as an initial condition for time-stepping. The normalised distance in phase space between this initial point and its evolution in time was then examined for local minima. Specifically, we define the scalar residual function

$$r_i(t > t_i) := \frac{|\boldsymbol{X}^{-\Delta z,-\Delta\theta}(t) - \boldsymbol{X}(t_i)|}{|\boldsymbol{X}(t_i)|} \tag{3.2}$$

where Δz is a distance by which the state $\boldsymbol{X}(t)$ is shifted back in z for comparison. We chose $\Delta z = L$ so that a value of $r_i(t) = 0$ for some $t > t_i$ means that the flow

in the pipe is *exactly* the flow at time t_i. In this case, $\boldsymbol{X}(t_i)$ lies on a periodic orbit of the system with the time interval $t - t_i$ being a multiple of the period (for $\Delta z \neq 0$, a vanishing residual would indicate a *relative* periodic orbit). For the ease of calculation we chose to neglect the possibility of recurrence occurring after a shift in the azimuthal direction θ, so $\Delta\theta = 0$ was imposed. Typical plots of $r_i(t)$ starting from different values of t_i are displayed in Figure 3. Every function r_i attains a smallest local minimum which is defined as

$$r_{min}(t_i) := \min_{t>t_i}\{\, r_i(t) \,|\, \frac{\partial r_i}{\partial t} = 0 \,\}. \tag{3.3}$$

The scalar function r_{min}, which can be determined for any given initial condition $\boldsymbol{X}(t_i)$, turns out to be the central quantity in this paper.

Figure 4 shows how r_{min} varies with the starting point. Our interpretation of Figure 4 is the following: phases for which r_{min} is low (below 0.1) correspond to approaches to periodic orbits of the system by the edge trajectory. Here, the alternating pattern of maxima and minima in r_{min} is the signature of a repellor - a set of states which attract trajectories to ultimately repel them away. For hyperbolic dynamical systems, trajectories are attracted towards one of these states along their stable manifold and ejected away along their unstable manifold (see the sketch in Figure 5). For the parameters here, 6 dips in the r_{min}-profile suggest 6 approaches, denoted respectively by $A1, B1, C1, D1, E1, F1$, to 6 different exact recurrent states. Parts of the trajectory linking one state to the next (e.g. $A1 \rightarrow B1$ or $D1 \rightarrow E1$) are located in the vicinity of heteroclinic connections between the two states, or homoclinic connections if two successive states are found to be similar. The notion of "vicinity" depends, of course, on the choice of the norm in phase space. Here, a pragmatic approach is adopted: we use the expression "$\boldsymbol{X}$ is close to a periodic orbit Y" to mean that the Newton-Krylov algorithm converges to the periodic orbit Y starting with the initial guess $\boldsymbol{X}$.

3.3. *Exact Coherent Structures in* Σ

We now analyse the neighbourhood of the points $\boldsymbol{X}(t_i)$ yielding a low value of r_{min} looking for exact recurrent states, for which r_{min} exactly vanishes. Starting from such initial guesses, we use the Newton-Krylov algorithm defined in §2.3 to minimise r_{min}. For the choice of the Euclidean norm in phase-space, convergence properties of Newton-like schemes ensure that the states to be found are *generally* in a neighbourhood of the starting point, i.e. that the edge trajectory from which the algorithm started actually approaches the states towards which it converged. We used the six different phases A to F of the previous subsection as starting guesses. Excellent convergence has been obtained in the cases $A1, B1, D1, F1$, where r_{min} was reduced to $O(10^{-11})$. The converged states are labelled respectively $A1\_0.625$, $B1\_0.625$, $D1\_0.625$ and $F1\_0.625$ in order to distinguish them from the starting points $A1, ..., F1$, and to indicate the parameter α. The cases $C1$ and $E1$ displayed only partial convergence to respectively $O(10^{-3})$ and $O(10^{-2})$ and it is not possible to say if there really are zeros of r_{min} in this neighbourhood. The initial guess might not have been good enough or there might only be a local positive minimum of the system corresponding to a nearly-recurrent state.

The converged states $A1\_0.625$, $B1\_0.625$, $D1\_0.625$ and $F1\_0.625$ all correspond to travelling wave solutions. Close inspection of their spatial structure and dynamics shows that they are all the *same* travelling wave solution modulo a shift in the azimuthal direction: see Figure 6. This "unique" state corresponds exactly to the "asymmetric" TW identified in Pringle & Kerswell (2007). Its z-averaged velocity field is also strongly rem-

iniscent of the chaotic state shown by Schneider et al. (2007). This resemblance has also been noted by Mellibovsky & Meseguer (2007) who used a different approach to infer the significance of this same asymmetric TW. Interestingly, the present study failed to find evidence that other states were approached for the chosen parameters in spite of the fact that other TWs are embedded in the edge. Using the same length of pipe, Kerswell & Tutty (2007) found that all four lower branch TWs they examined lie in Σ: a turbulent transient was initiated when the TW was perturbed along its most unstable eigendirection in one sense, whereas swift relaminarisation occurred for the other. The most likely explanation is that these other TWs, all of which fitted at least two full wavelengths in the pipe, are much more unstable and hence far less frequently visited.

The search for recurrent states described above was initially undertaken with $\Delta\theta = 0$ disallowing azimuthal propagation of the recurrent patterns. In the case $A1$, we experimented with allowing $\Delta\theta$ to be updated by the Newton-Raphson scheme. This involved solving an additional equation $\partial g/\partial\Delta\theta = 0$ (Viswanath 2007a). Using Newton-Raphson with the same starting guess $A1$ but allowing the shift $\Delta\theta$ to be updated, produced convergence to another state $A'\_0.625$ distinct from $A1\_0.625$. This state, despite a velocity profile very analogous to that of $A1\_0.625$, rotates by an angle $\Delta\theta = -0.32$ degrees after travelling one pipe length. This situation is very reminiscent of the bifurcation diagram obtained by Pringle & Kerswell (2007) for the asymmetric TW (though here Re is much higher): for a given Reynolds number, a branch of solutions with helicity is connected to the mirror-symmetric branch, and intersects the non-helical subspace twice. The solutions at the crossing points are non-helical but nevertheless possess a rotational propagation speed $c_\theta \neq 0$, like our solution $A'\_0.625$. The fact that such a solution has been found here could be explained by the fact that the numerical code used does not allow helicity, hence the Newton-Raphson algorithm has no choice but to look for the intersection of the helical branch with a non-helical subspace. However, other attempts to find exact recurrent patterns with rotation invariably converged back to a non-rotating $\Delta\theta = 0$ TW.

3.4. *Search for Heteroclinic Connections*

The results so far indicate the possible existence of heteroclinic trajectories linking the exact states found. When the two successively visited states are the same modulo a shift in the azimuthal direction, "relative" homoclinic connection is a more appropriate term. Though such connections, if they exist, need an infinite time to occur, we try to locate them by carefully chosing a trajectory starting in the vicinity of a TW. The asymmetric travelling wave of Pringle & Kerswell (2007) was chosen (i.e. $A1\_0.625$) with the parameters $(\alpha, Re, m_0) = (0.625, 2875, 1)$ and orientated so that it was symmetric around the $\theta = 0$ plane. In the corresponding S-symmetric subspace, the solution has exactly two unstable eigendirections, denoted by $\boldsymbol{e}_1$ and $\boldsymbol{e}_2$, $\boldsymbol{e}_1$ being the most unstable one (there are no unstable directions in the dual space). These two vectors are normalised so that their energy norm is unity. We now define a starting point by

$$\boldsymbol{X}(0) = \boldsymbol{X}_{TW} + \epsilon\left(\cos\phi\,\boldsymbol{e}_1 + \sin\phi\,\boldsymbol{e}_2\right). \tag{3.4}$$

In this expression, ϵ is a small positive parameter which ensures that the dynamics near $\boldsymbol{X}(0)$ is closed to the tangent unstable eigenspaces of the exact solution, i.e. the dynamics is linear ($\epsilon = 10^{-2}$ suffices). The angle ϕ defines a plane spanned by $\boldsymbol{e}_1$ and $\boldsymbol{e}_2$ and vanishes in the direction of $\boldsymbol{e}_1$. For some values of the angle ϕ, the trajectory starting from $\boldsymbol{X}(0)$ returns quickly to the laminar state, whereas for some other angles, it becomes turbulent. This demonstrates that $\boldsymbol{X}_{TW}$ itself also sits on the edge Σ. In

both cases the trajectory starts in the S-symmetric subspace, but after a finite time this symmetry is broken. A bisection method is used to determine (to machine precision) an angle ϕ for which the trajectory neither evolves to the laminar or turbulent state (see Figure 7 for a sketch of the method). The energy contained in the axially-dependent modes is displayed in Figure 8 and the residual function $r_{min}(t)$ in Figure 9. These show that r_{min} increases exponentially and the energy stays constant until $t \sim 150D/U$. After this linear regime, r_{min} increases, before dropping to a value of 0.09 at $t \sim 250D/U$ and then increasing again. The flow at this local minimum of r_{min} does not resemble any of the known states. However, when used as a starting point for the Newton-Raphson algorithm, r_{min} smoothly decreases to $O(10^{-11})$. The exact solution happens to be the asymmetric travelling wave again, but shifted by an angle of 51.56 degrees. This suggests the existence of a relative homoclinic connection.

3.5. Σ *under* R_2*-Symmetry*

The technique developed above to identify recurrent states in the edge can equally be applied to the dynamics within a symmetry subspace. Restricting the flow to be R_m-symmetric, for example, improves the possibility of an edge trajectory coming close to some of the R_m-symmetric lower branch TWs found in Wedin & Kerswell (2004) and thereby confirming their presence in the edge. There is also, of course, the possibility of discovering unknown branches of TWs. Attention was restricted to the R_2-symmetric subspace by setting $m_0 = 2$ in the flow representation (2.4). At $Re = 2875$, $\alpha = 0.625$ and resolution $(15, 30, 15)$, a chaotic edge trajectory was followed for $O(500\,D/U)$ during which 5 different phases of relative recurrence - labelled $A2, B2, C2, D2$ and $E2$ - were detected. Interestingly, this edge trajectory, although chaotic, is much smoother than the corresponding (same Re and α) edge trajectory for $m_0 = 1$: compare Figures 1 and 10. Of the 5 initial conditions for a Newton-Raphson search, r_{min} converged to $O(10^{-11})$ for only $D2$ and $E2$ (r_{min} for $A2, B2$ and $C2$ stagnated at $O(10^{-3})$). The exact recurrence states found, labelled $D2\_0.625$ and $E2\_0.625$ (see Figure 11), correspond to two new travelling wave branches distinct from those reported in Faisst & Eckhardt (2003) and Wedin & Kerswell (2004).

3.6. *Local Attractors within the* R_2*-Symmetric Subspace*

In this subsection, the flow is again restricted to be R_2-symmetric but the pipe is halved in length $\alpha = 1.25$ and Re reduced to 2400 (resolution is $(50, 16, 20)$). At these settings, Kerswell & Tutty (2007) found a lower branch TW, called $2b\_1.25$, which is on the edge and only has one unstable direction normal to the edge. This TW is therefore a local attractor for trajectories confined to the edge. The question is whether it is also a global attractor.

A starting point was randomly chosen along a turbulent trajectory, and an edge trajectory generated for $500\,D/U$ using the method described above. The energy signal is displayed in Figure 12 and the corresponding recurrence signal $r_{min}(t)$ is displayed in Figure 13. Two successive dips in r_{min} can be seen at times $50\,D/U$ and $90\,D/U$ later corresponding to inexact recurrences labelled respectively $A3$ and $B3$. When used to initialise a Newton-Raphson search, both lead to a value of $O(10^{-11})$ for r_{min}. The two converged exact states correspond to one unique travelling wave solution, differing only by a small shift (in the azimuthal direction) of less than 4 degrees. As a result, we label only the first $A3\_1.25$: see Figure 11. The trajectory evidently visits $A3$, leaves its neighbourhood and later approaches $B3$. The TW $A3\_1.25$ has an interesting structure made of 4 low-speed streaks near the walls separated by 4 high-speed streaks. Four other

high-speed streaks of lesser amplitude and smaller size, and with a much more steady structure, can be found closer to the pipe axis. This new TW thus has a richer structure than the $m_0 = 2$ branch of solution found in Faisst & Eckhardt (2003) and Wedin & Kerswell (2004).

After a time $200\,D/U$, the energy of the edge trajectory reaches a constant plateau and the value of r_{min} decreases exponentially to $O(10^{-4})$ by $300\,D/U$. This indicates that the trajectory is converging to an end state. Newton-Raphson can be used to accelerated the convergence of the trajectory by taking the state at $300\,D/U$ and reducing r_{min} to $O(10^{-11})$. The spatial structure of the initial flow at $300\,D/U$ and the final converged state, however, is indistinguishable. The final state is yet another new travelling wave solution, labelled $C3\_1.25$ (see Figure 11), distinct from TW $2b\_1.25$ of Kerswell & Tutty (2007). Stability analysis of $C3\_1.25$ reveals only one unstable direction which has to be normal to the edge. Hence $C3\_1.25$ is an attractor in the edge, and both $C3\_1.25$ and $2b\_1.25$ can only be local attractors.

4. Discussion

We first start by summarising the findings of this investigation.

- The laminar-turbulent boundary Σ in a short pipe has a chaotic attractor as found by Schneider et al. (2007).
- Although Σ is believed to have many unstable lower branch TWs embedded in it (Kerswell & Tutty 2007), only evidence for the asymmetric TW (Pringle & Kerswell 2007) and derivatives of it were found.
- A new asymmetric TW which has a small but finite azimuthal phase speed has been discovered.
- Evidence for a "relative" homoclinic connection was found between the asymmetric TW and the same wave with a different orientation.
- Calculations within a R_2-symmetric subspace have revealed new branches of R_2-symmetric TW solutions.
- The laminar-turbulent boundary restricted to R_2-symmetry has at least two simple local attractors in the form of TWs at $Re = 2400$.

Our numerical experiments have shed some light on the dynamical structure of Σ in pipe flow. When no symmetry is imposed, and the pipe is approximately $5\,D$ long ($\alpha = 0.625$), trajectories which neither relaminarise nor become turbulent are all chaotic and visit some exact recurrent states in a transient manner. In all cases studied, these exact solutions appear to be the asymmetric TWs found by Pringle & Kerswell (2007) even though many other lower branch TWs are embedded in Σ (Kerswell & Tutty 2007). No RPOs were found even though the numerical method was originally designed to find them. Whether this is because the RPOs are rarely visited or just more difficult to isolate is unclear. It is tempting to conclude that the edge of chaos of pipe flow is structured around a set of unstable saddle points (the TWs) linked together by heteroclinic or sometimes relative heteroclinic connections. An approximation to such a connection has been shown in §3.4. The resulting dynamical structure is likely to be a heteroclinic (or homoclinic) tangle, an efficient mechanism to produce chaotic trajectories in phase-space with the set of TWs acting as a skeleton of the tangle. Seen from this point of view, transition to turbulence from a given initial condition depends on the position of the initial state, in phase space, relative to the stable manifold of each exact state embedded in Σ. When a trajectory approaches a travelling wave solution belonging to Σ, its relative position to

TW	m_0	Re	C	c_θ	status
$A1\_0.625$	1	2875	1.55494	0	known
$A'\_0.625$	1	2875	1.51956	$-1.704.10^{-3}$	new
$D2\_0.625$	2	2875	1.53382	0	new
$E2\_0.625$	2	2875	1.57350	0	new
$A3\_1.25$	2	2400	1.23818	0	new
$C3\_1.25$	2	2400	1.55064	0	new

TABLE 1. Parameters, axial propagation speed C (in units of U) and azimuthal propagation speed c_θ in $radU/D$ and status of all travelling wave solutions found in this paper.

the boundary determines on which side of the edge the trajectory escapes, resulting in either relaminarisation or a turbulent transient (see sketch in Figure 5).

When the flow is artificially restricted to be R_2-symmetric at $Re = 2875$, the trajectory remains chaotic but it visits various *distinct* TW states ($D2\_0.625$ and $E2\_0.625$) By halving the pipe length to $\approx 2.5D$ and reducing Re to 2400, multiple local attractors appear in Σ. A randomly started trajectory, after a chaotic transient and a visit to the states $A3\_1.25$ and $B3\_1.25$, is attracted towards the TW solution $C3\_1.25$. The fundamental difference between $C3\_1.25$ and all the other states approached so far lies in the number of unstable eigenvalues. When a TW has got two or more unstable eigenvalues in a given subspace, the dimension of the intersection between its unstable manifold and the hypersurface Σ is reduced by one but remains at least one. Hence such a state remains a saddle point on Σ: edge trajectories enter its vicinity along its stable manifold and escape along the unstable manifold. In contrast, when a state has only one unstable direction, this is necessarily normal to Σ, so that the state becomes an attractor for dynamics *restricted to the edge*. We have shown that $C3\_1.25$ is one such TW, but there is at least another labelled $2b\_1.25$ (Kerswell & Tutty 2007). Therefore we expect both these two states to be only *local* attractors on Σ rather than global ones. In the cases of plane Poiseuille and Couette flow, a lower-branch solution exists which has only one unstable direction and is therefore a local attractor on the edge (Toh & Itano 1999, 2001, Lagha et al., 2008). The case of pipe flow is different since TWs all seem to have at least two unstable directions when there is no imposed discrete rotational symmetry. For example, the $2b\_1.25$ TW has 1 harmonic (R_2-symmetric) unstable eigenfunction and one subharmonic (only R_1-symmetric) unstable eigenfunction.

Although artificial, discrete rotational symmetry constraints have been a useful device for discovering new exact recurrent solutions. The transient nature of the repellor found on Σ demonstrates the fact that by choosing appropriate initial conditions, a large number of potentially new states is visited in a finite time (see Table 1). The method developed here based on edge tracking, recurrence analysis and use of a Newton-Krylov algorithm, is a very general approach to discover new exact recurrent solutions in any flow situation possessing subcritical behaviour. Importantly, the present method naturally selects the states that are most likely to be visited and does not presuppose anything about their spatial structure (modulo the symmetries imposed on the flow). The use of the scalar function r_{min}, coupled with a Newton-Krylov solver, can also be used to search for more

complex solutions like relative periodic orbits, whether located on the laminar-turbulent boundary or embedded in fully developed turbulence. This is currently underway.

Many open questions remain regarding Σ in pipe flow. Firstly, is Σ really a hypersurface or can it have a more fractal structure? Why does the flow keep reapproaching the asymmetric TW or rotations of it, and not any of the other lower branch TWs known to exist within the same parameters range? Finally, what does Σ look like in longer pipes where localised turbulent structures called "puffs" exist? Preliminary work in a reduced model has already revealed an interesting localised structure as the attracting state (Willis & Kerswell 2008).

Acknowledgements:

We would like to thank Chris Pringle for helping with the velocity profiles of the TW solutions and Bruno Eckhardt for stimulating discussions about this topic. Y.D. is supported by a Marie-Curie IntraEuropean Fellowship (grant number MEIF-CT-2006-024627) and A.W. by the EPSRC (grant number GR/S76144/01).

REFERENCES

Dennis, J. E. Jr. & Schnabel, R. E. 1995 *Numerical Methods for Unconstrained Optimization and Nonlinear Equations*, *SIAM*

Eisenstat, C. & Walker, H. 1996 Choosing the forcing terms in an inexact Newton method *SIAM J. Sci. Comput.*, **17**, 16-32

Faisst, H. & Eckhardt, B. 2003 Travelling waves in pipe flow *Phys. Rev. Letters*, **91**,224502

Faisst, H. & Eckhardt, B. 2004 Sensitive dependence on initial conditions in transition to turbulence *J. Fluid Mech.*, **504**, 343-352

Hagen, G. H. L. 1839 Uber die Bewegung des Wassers in engen zylindrischen Rohren *Poggendorfs Annalen der Physik und Chemie*, **16**, 423

Hof, B., van Doorne, C. W. H., Westerweel, J., Nieuwstadt, F. T. M., Faisst, H., Eckhardt, B., Wedin, H., Kerswell, R.R. & Waleffe, F. 2004 *Science*, **305**, 1594-1597

Hof, B., Westerweel, J., Schneider, T. & Eckhardt, B. 2006 Finite lifetime of turbulence in shear flows *Nature*, **443**, 59

Itano, T. & Toh, S. 2001 The dynamics of bursting process in wall turbulence *J. Phys. Soc. Japan* **70**, 703-716

Joseph, D. D. & Carmi, S. 1969 Stability of Poiseuille flow in pipes, annuli, and channels *Quart. Appl. Math.*, **26**, 575-599

Kawahara, G. 2005 Laminarization of minimal plane Couette flow: Going beyond the basin of attraction of turbulence *Phys. Fluids*, **17**, 041702

Kerswell, R. R. 2005 Recent progress in understanding the transition to turbulence in a pipe *Nonlinearity*, **18**, R17-R44

Kerswell, R. R. & Tutty, O.R. 2007 Recurrence of Travelling Waves in Transitional Pipe Flow *J. Fluid Mech.*, **584**, 69-102

Lagha, M., Schneider, T., De Lillo, F. & Eckhardt, B. 2008 Laminar-turbulent boundary in plane Couette flow *preprint*

Marqués, F. 1990 On boundary conditions for velocity potentials in confined flows: Application to Couette flow *Phys. Fluids*, **A2** , 729-737

Mellibovsky, F. & Meseguer, A. 2007 Pipe flow dynamics on the critical threshold *Proceedings of the 15th Int. Couette-Taylor Workshop* (ed. Mutabazi, I.), Le Havre, France

Peixinho, J. & Mullin, T. 2006 Decay of turbulence in pipe flow *Phys. Rev. Lett.*, **96**, 094501

Peixinho, J. & Mullin, T. 2007 Finite-amplitude thresholds for transition in pipe flow *J. Fluid Mech.*, **582**, 169-178

Pfenniger, W. 1961 Transition in the inlet length of tubes at high Reynolds numbers *Boundary Layer and Flow Control* (ed. GV Lachman), **970**

Poiseuille, J. L. M. 1840 Recherches experimentales sur le mouvement des liquides dans les tubes de très petits diamètres *C.R. Acad. Sci.*, **11**, 961

Pringle, C. C. T. & Kerswell, R. R. 2007 Asymmetric, helical and mirror-symmetric travelling waves in pipe flow *Phys. Rev. Letters*, **99**, 074502

Reynolds, O. 1883 An experimental investigation of the circumstances which determine whether the motion of water shall be direct or sinuous and of the law of resistance in parallel channels *Phil. Trans. Roy. Soc.*, **174**, 935-982

Saad, Y. & Schultz, M.H. 1986 GMRES: a generalized minimal residual method for solving nonsymmetric linear systems *Siam J. Sci. Stat. Comput*, **7**, 856-869

Schneider, T. M., Eckhardt, B. & Yorke, J. A. 2007 Turbulence transition and the edge of chaos in pipe flow *Phys. Rev. Lett.*, **99**, 034502

Skufca, J.D., Yorke, J. A. & Eckhardt, B. 2006 Edge of Chaos in a Parallel Shear Flow *Phys. Rev. Letters*, **96**, 174101

Toh, S. & Itano, T. 1999 Low-dimensional dynamics embedded in a plane Poiseuille flow turbulence: Traveling-wave solution is a saddle point? *Proc. IUTAM Symp. on Geometry and Statistics of Turbulence* (ed. Kambe, T.), Kluwer

Toh, S. & Itano, T. 2003 A periodic-like solution in channel flow *J. Fluid Mech.* **481**, 67-76

Viswanath, D. 2007 The dynamics of transition to turbulence in plane Couette *preprint* http://www.arxiv.org/abs/physics/0701337

Viswanath, D. 2007 Recurrent motions within plane Couette turbulence *J. Fluid Mech.*, **580**, 339-358

Wedin, H. & Kerswell, R. R. 2004 Exact coherent structures in pipe flow: travelling wave solutions *J. Fluid Mech.*, **508**, 333-371

Willis, A. P. & Kerswell, R. R. 2007 Coherent structures in local and global pipe turbulence *submitted* http://www.arxiv.org/abs/0706.3330

Willis, A. P. & Kerswell, R. R. 2008 Turbulent dynamics of pipe flow captured in a reduced model: all of the behaviour at a fraction of the cost. *preprint*

Wygnanski, I. J., Champagne, F. H. 1973 On transition in a pipe. Part 1. The origin of puffs and slugs and the flow in a turbulent slug *J. Fluid Mech.*,**59**, 281

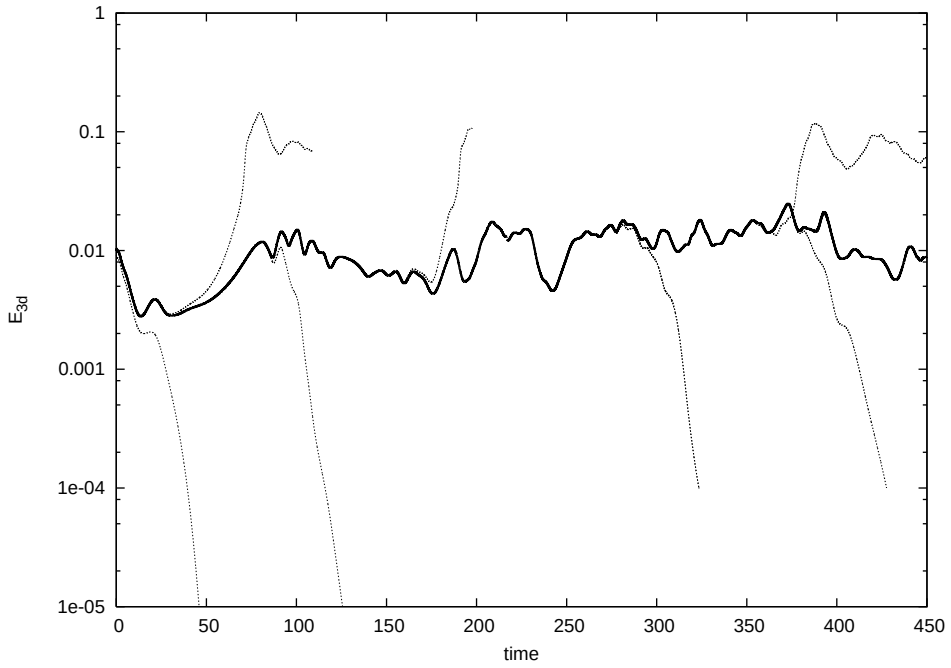

FIGURE 1. Energy contained in the axially-dependent modes for $(\alpha, Re, m_0) = (0.625, 2875, 1)$. The thick line indicates the edge trajectory and the thinner lines nearby trajectories which either relaminarise (energy decreases) or becomes turbulent (energy increases to a higher level). Time is in units of D/U.

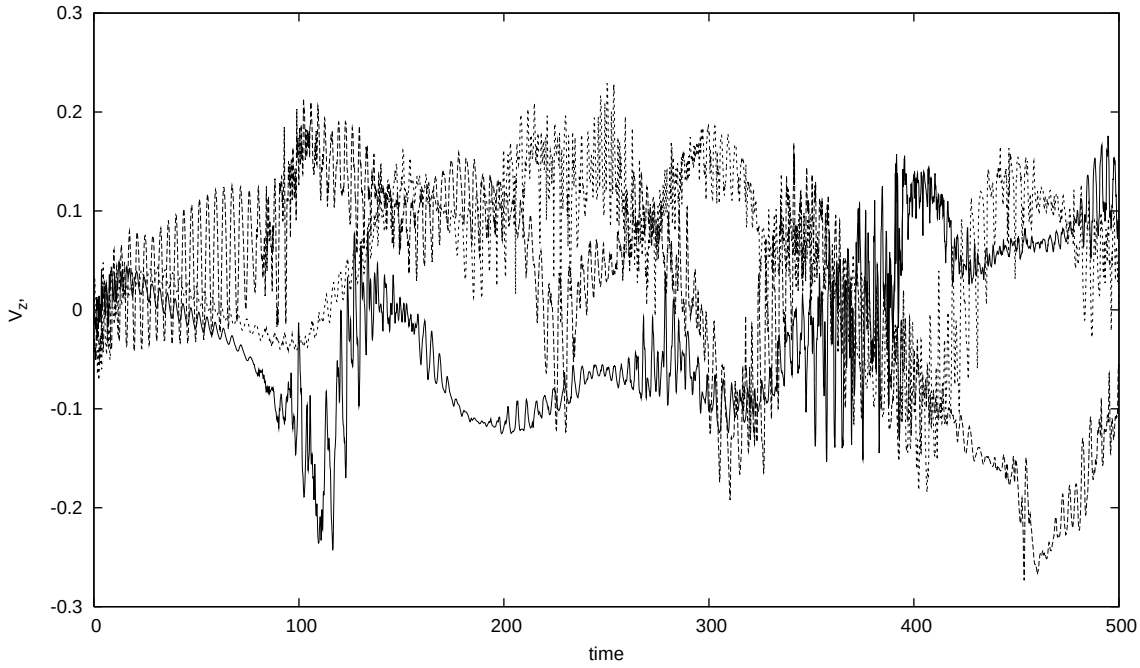

FIGURE 2. Axial perturbation velocity signal at three different locations in the pipe. The signal is taken from the edge trajectory of §3.1.

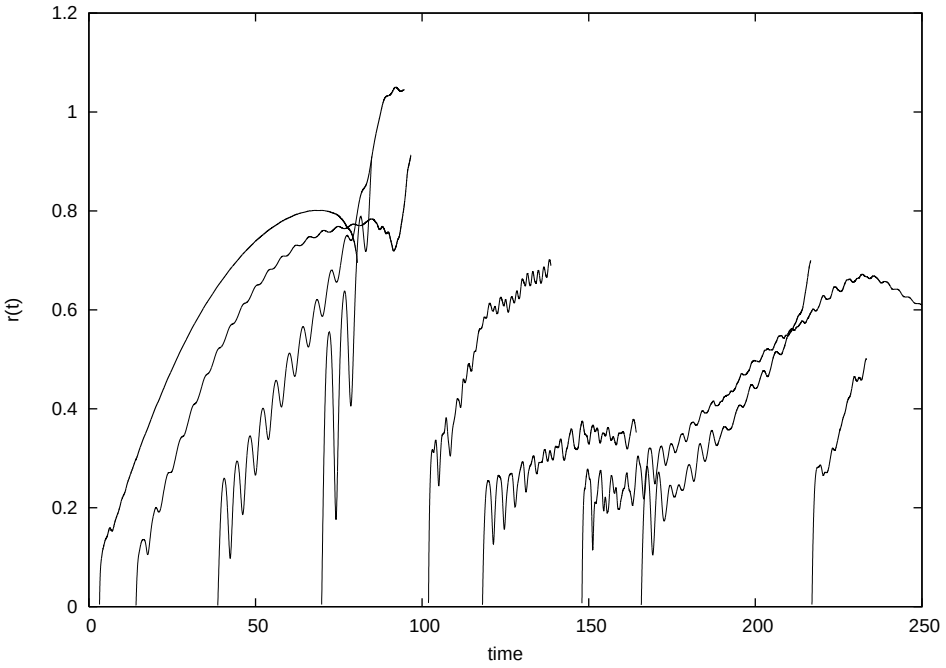

FIGURE 3. Typical profiles of the residual function $r(t)$ starting from snapshots of the edge trajectory of Section 3.1. The subscript i has been suppressed (time in units of D/U).

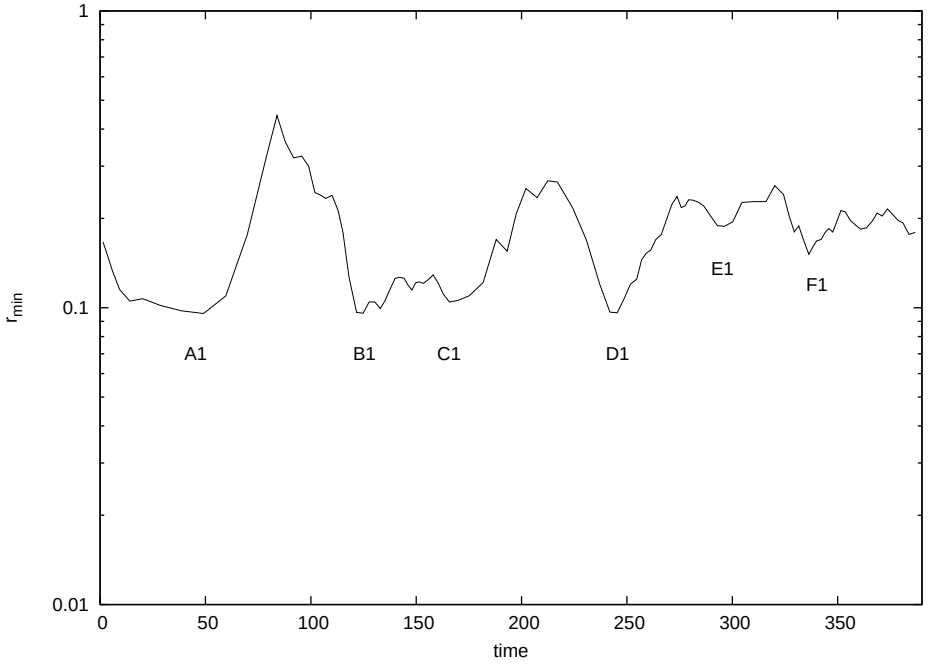

FIGURE 4. Recurrence signal for the edge trajectory of Section 3.1 (for definition of r_{min} see text) against time in D/U. $(\alpha, Re, m_0) = (0.625, 2875, 1)$.

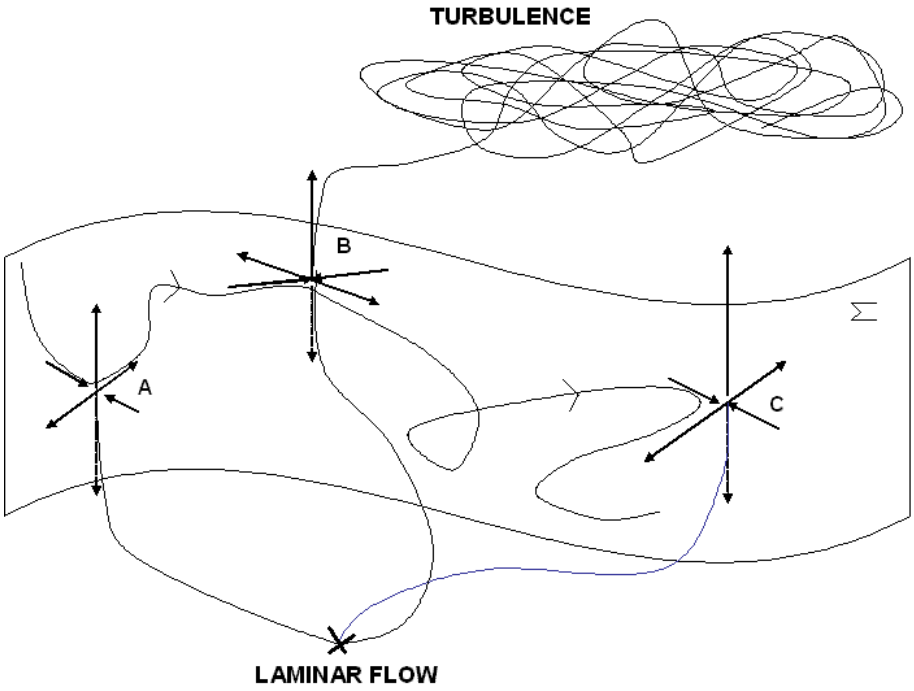

FIGURE 5. Schematic view of phase-space. The surface Σ separates initial conditions which relaminarise from those which become turbulent. An edge trajectory visiting three states A, B and C is shown schematically. The dynamics on the manifolds transverse to Σ are shown by trajectory diverging towards either the laminar state or the turbulent state.

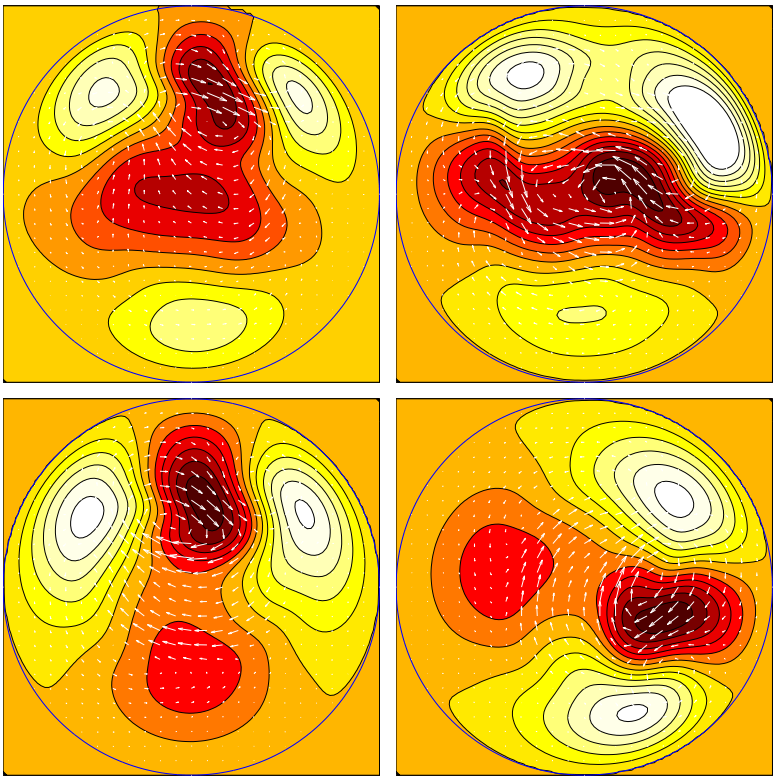

FIGURE 6. Starting guesses for the Newton-Krylov algorithm (top left $A1$, top right $B1$) and converged states (bottom left $A1_0.625$, bottom right $B1_0.625$) on the edge trajectory described in §3.2. Each subfigure represents a snapshot across the pipe. Contours indicate the axial velocity difference from the underlying laminar flow (light/dark indicating faster/slower moving fluid) and the arrows represent the cross-stream velocity (length proportional to speed magnitude). Maximum norm of the (u, v) cross-velocity is $0.0128U$ and the axial velocity differential w is in the range $\pm 0.17U$. The TWs $A1\_0.625$ and $B1\_0.625$ are exactly the same state modulo an azimuthal shift.

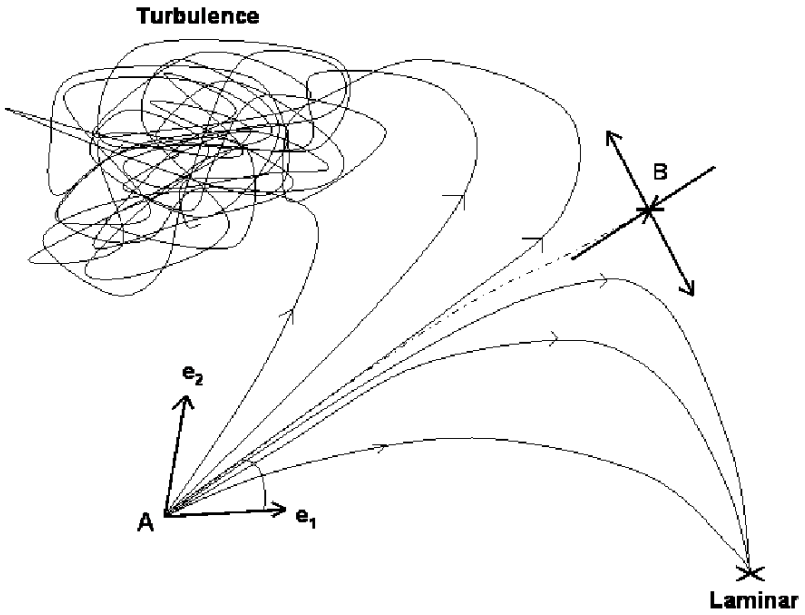

FIGURE 7. A sketch of the heteroclinic connnection joining two saddle points A and B. $\boldsymbol{e}_1$ and $\boldsymbol{e}_2$ are the two unstable eigendirections of A, used for shooting by varying the shooting angle, in order to optimise the approach to B.

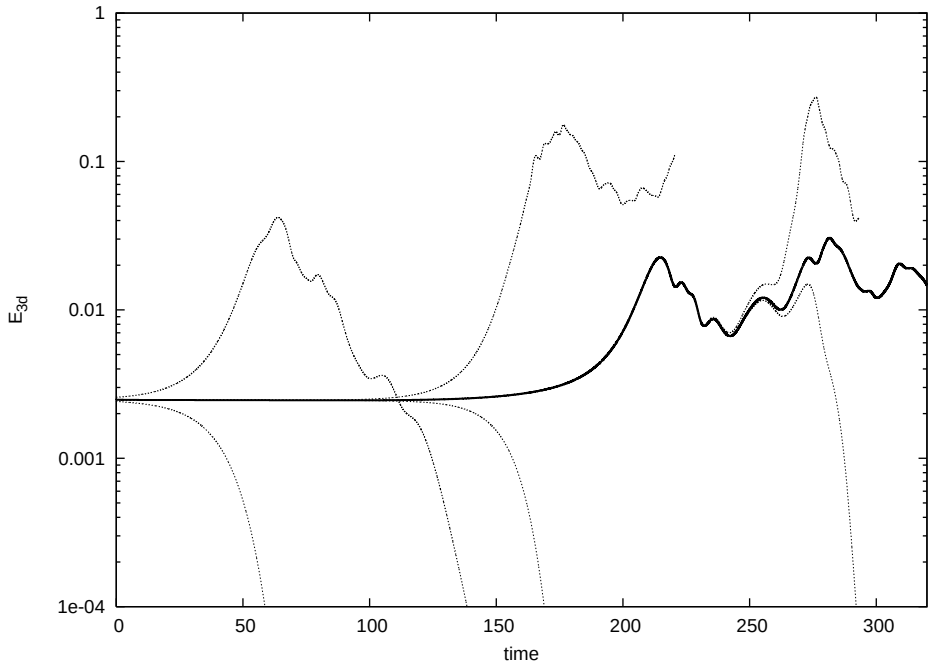

FIGURE 8. Energy contained in the axially dependent modes for $Re = 2875$, $m_0 = 1$, $\alpha = 0.625$. The thick line indicates the edge trajectory and the thinner lines nearby trajectories which either relaminarise (energy decreases) or becomes turbulent (energy increases to a higher level). Time is in units of D/U

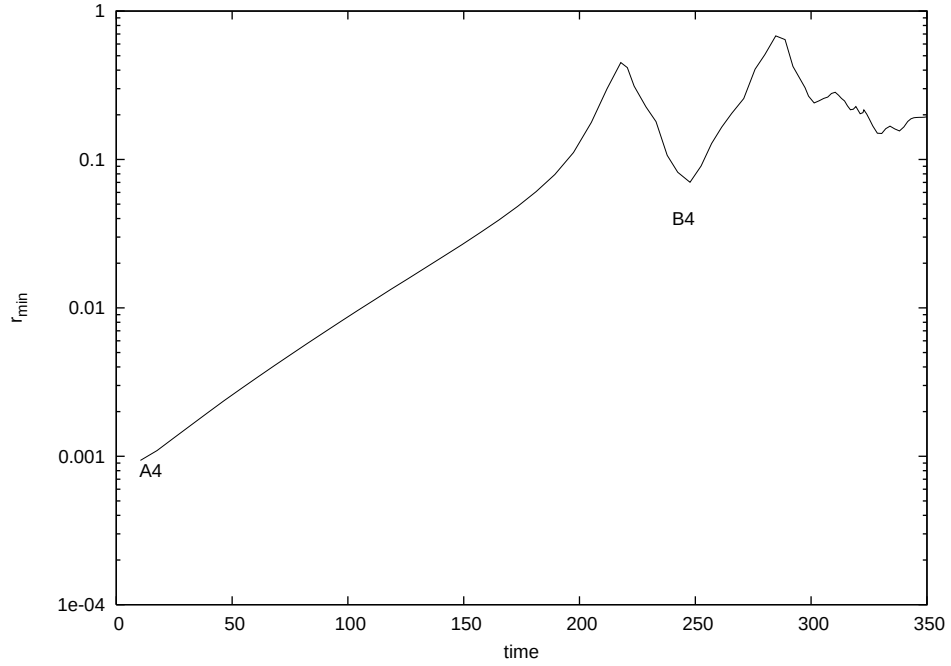

FIGURE 9. Recurrence signal for the heteroclinic connection of §3.4 versus time (in D/U). $(\alpha, Re, m_0) = (0.625, 2875, 1)$.

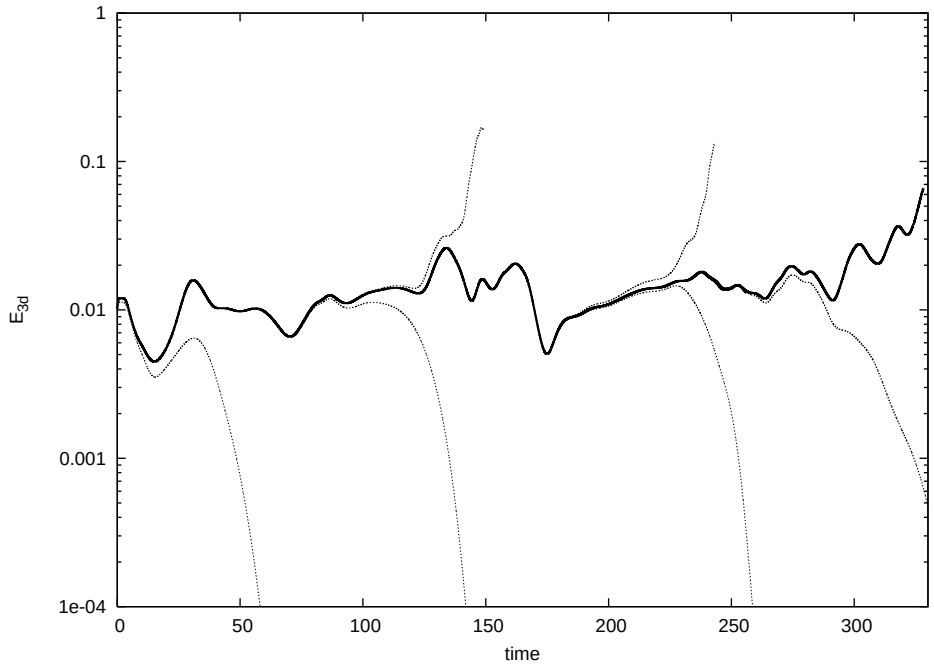

FIGURE 10. Energy contained in the axially-dependent modes on the edge for $(\alpha, Re, m_0) = (0.625, 2875, 2)$. The thick line indicates the edge trajectory and the thinner lines nearby trajectories which either relaminarise (energy decreases) or becomes turbulent (energy increases to a higher level). Time is in units of D/U

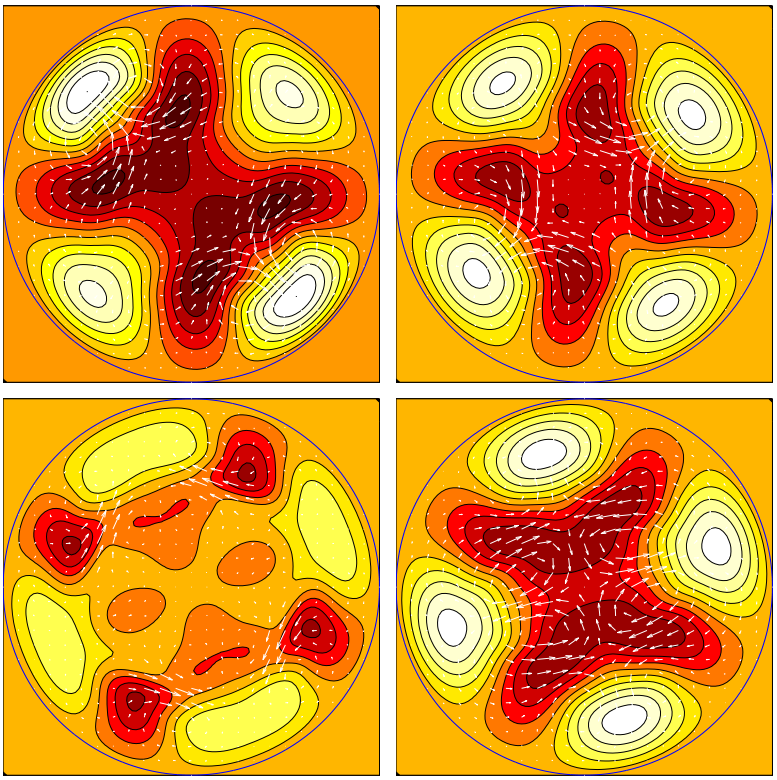

FIGURE 11. Converged states $D2\_0.625$ (top, left), $E2\_0.625$ (top, right), $A3\_1.25$ (bottom, left) and $C3\_1.25$ (bottom,right). Contours indicate the axial velocity difference from the underlying laminar flow (light/dark indicating faster/slower moving fluid) and the arrows represent the cross-stream velocity (length proportional to speed). Across the four snapshots, the maximum speed of cross-velocity is $0.0143U$, axial velocity w is in the range $\pm 0.17U$.

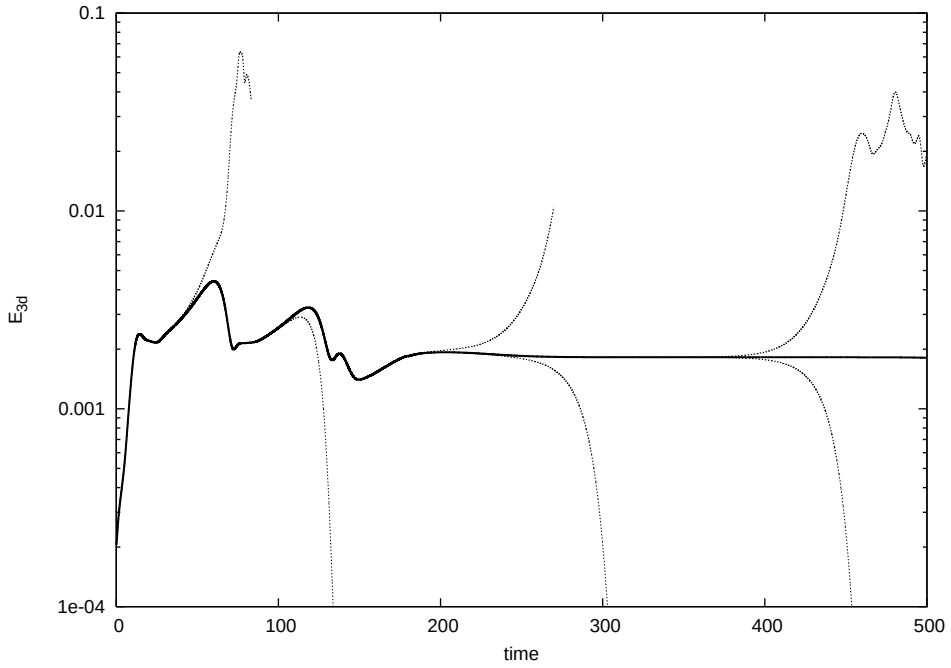

FIGURE 12. Energy contained in the axially-dependent modes for $(\alpha, Re, m_0) = (1.25, 2400, 2)$. The thick line indicates the edge trajectory and the thinner lines nearby trajectories which either relaminarise (energy decreases) or becomes turbulent (energy increases to a higher level). Time is in units of D/U

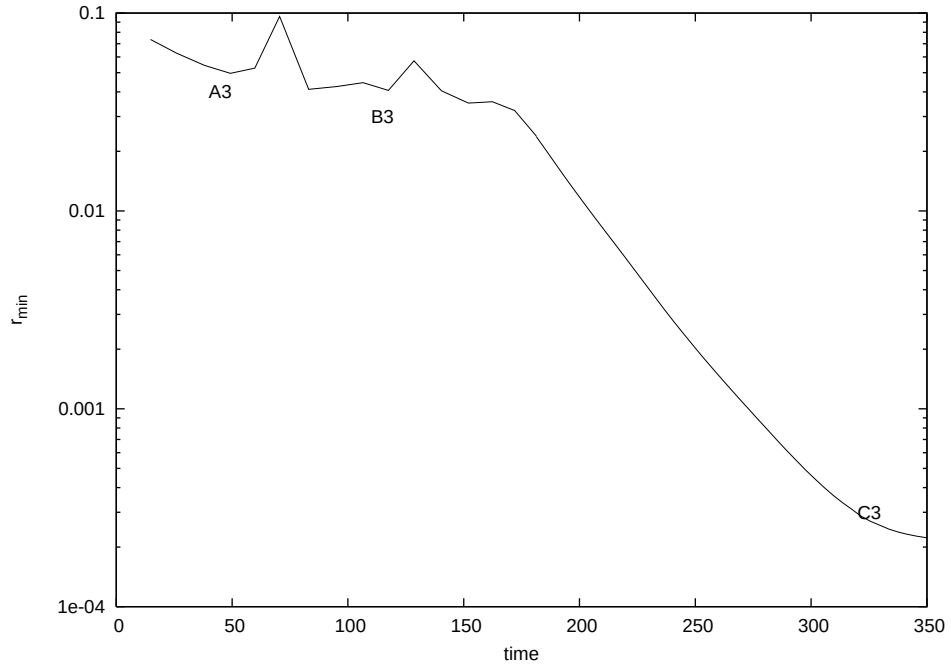

FIGURE 13. Recurrence signal for the attracting state of Section 3.5 versus time expressed in D/U units. $(\alpha, Re, m_0) = (1.25, 2400, 2)$.